Traveling-wave convection in colloids stratified by gravity

B. L. Smorodin,[1,*] I. N. Cherepanov,[1] B. I. Myznikova,[2] and M. I. Shliomis[3]

[1]*Perm State University, 15 Bukirev Street, 614990 Perm, Russia*

[2]*Institute for Continuum Mechanics, Urals Branch of Russian Academy of Sciences, 1 Academician Korolyov Street, 614013 Perm, Russia*

[3]*Department of Mechanical Engineering, Ben-Gurion University of the Negev, P.O Box 653, Beer-Sheva 84105, Israel*

(Received 16 February 2011; revised manuscript received 12 June 2011; published 8 August 2011)

Thresholds of convection excitation and nonlinear convective flow patterns in a horizontal colloidal-mixture layer heated from below are investigated. We take into consideration the fact that, provided the barometric stratification has been reached prior to imposing the temperature gradient, only oscillatory disturbances develop. The influence of separation ratio, sedimentation length, and Prandtl number on the thresholds of oscillatory convection is studied. To examine the complex nonlinear dynamics of the system, numerical simulations with realistic boundary conditions have been carried out using a finite difference method. Long-wave and cellular instability modes as well as transitions between the conductive state and the traveling-wave regime are discussed. It is shown that the traveling-wave regime is stable within a specified range of heating intensity (the Rayleigh number interval). Complex bifurcation and spatiotemporal properties of dissipative structures caused by the interaction of the gravity-induced concentration gradient, nonlinear advection, and mixing of the fluid with nanoparticles are considered.

DOI: 10.1103/PhysRevE.84.026305 PACS number(s): 47.20.Ky, 47.55.P−, 47.54.−r

I. INTRODUCTION

A majority of dynamical processes occurs in multiphase systems, and it is no wonder that contemporary continuum mechanics problems involve the study of volumetrically coupled phenomena in compositions of materials with different physical properties,which coexist and operate within the same spatial regions. During the past decade, progress in understanding the effects accompanying flows of solid particles suspended in a continuous liquid medium has been achieved through the results of numerous investigations. These efforts are important for fundamental science focusing on description, simulation, design, and control of processes in colloids, as well as for multiple applications of colloidal mixtures in chemical, pharmaceutical, food, cosmetic, wastewater, and other industries, medical technology, bioprocessing, and environmental engineering [1,2].

A colloidal mixture contains dispersed-phase particles which are about 10–100 nm in diameter. Similarly to the instability phenomenon observed in one of the most investigated heat transfer problems (the Rayleigh-Benard problem) for molecular binary mixtures [3–11], in a colloid-mixture layer under gravity segregation [13] there may be density inhomogeneity, and consequently, the volume force, which depends on thermal conditions and solid phase distribution. Thermal diffusion (the Ludwig-Soret effect) in turn influences the relationship between the concentration and temperature fields and the bifurcations in colloidal systems. The large difference between the characteristic times of thermal and diffusive processes is the cause of the interesting properties of convection in colloidal suspensions [12–17].

A large number of spatiotemporal patterns has been observed in the convective flows of binary mixtures with negative Soret coupling. The specific directed motion of a heavy component to a hot boundary of the layer weakens the buoyancy effect and gives rise to growing oscillatory disturbances, whose nonlinear evolution generates a variety of regimes. In colloidal mixtures, another segregation mechanism exists; the heavy component migrates in the direction opposite to gravity. Depending on initial conditions, the onset of convection may be related to the development of monotonic or oscillatory instability modes [13]. Oscillations in the colloidal mixture have been experimentally observed over a long time interval (within approximately a week) [17].

This paper presents the results of a theoretical study of convection in a horizontal layer filled with a suspension of solid nanoparticles in an incompressible viscous fluid stratified under terrestrial conditions. In Sec. II, we focus on a proper mathematical formulation of nonisothermal processes in a two-component system with thermal diffusion and sedimentation, in which mechanical equilibrium may be unstable. In Sec. III, the linear theory of convective instability is developed to analyze the behavior of the colloid fluid system. In Sec. IV, linear analysis of the normal mode of perturbations is extended to include the study of nonlinear evolution of perturbations. We use the obtained numerical results to analyze the developed convection regimes and to describe the oscillatory transitive dynamics of the system and the stable traveling-wave regime. In Sec. V, the results of the research are summarized.

II. GOVERNING EQUATIONS

We consider a horizontal, colloid-mixture layer placed in the gravitational field of the Earth. The layer is bounded by rigid, perfectly heat-conducting and impermeable parallel planes located at $z = 0$ and $z = h$ (h is the layer thickness). The temperature T_u of the upper boundary as well as the temperature T_l of the lower boundary are fixed. The temperature difference is denoted by ΔT. We assume that all transfer coefficients, like the diffusion coefficient D, temperature diffusivity coefficient κ, and coefficient of fluid viscosity η, are constants.

*bsmorodin@yandex.ru

Let the colloid mixture be a suspension of grains with diameter d, the mean volume fraction $\overline{C}$, and density ρ_s in a carrier liquid of density ρ_f. The equilibrium grain concentration in conductive state that is maintained in the large depth layer in the gravitational field obeys the barometric formula

$$C_{\rm cond}(z) = C_* e^{-z/l_{\rm sed}}, \quad l_{\rm sed} = k_B T/(\Delta\rho V g), \tag{2.1}$$

where C_* is the concentration on the lower boundary of the layer, $\mathbf{g}$ is the gravity acceleration, $l_{\rm sed}$ stands for the *sedimentation length*, $\Delta\rho = \rho_s - \rho_f$, and V denotes the particle volume; the z axis is directed upward. All estimates are carried out for a water-based suspension of silica ($\rho_s = 2.255$ g/cm^3, $d = 22$ nm) examined earlier in [12,13]. The data yields the spatial scale of sedimentation $l_{\rm sed} \simeq 60$ mm. For the layer of thickness $h = 2$ mm, the ratio $h/l_{\rm sed} \simeq 1/30$ is sufficiently small, so it is reasonable to replace the barometric distribution (2.1) by the linear one,

$$C_{\rm cond}(z) \simeq C_*(1 - z/l_{\rm sed}), \tag{2.2}$$

implying that the concentration gradient through the layer is almost constant and the mean concentration $\overline{C}$ slightly differs from value C_*:

$$dC_{\rm cond}(z)/dz \simeq -C_*/l_{\rm sed}, \tag{2.3}$$

$$\overline{C} = \frac{1}{h}\int_0^h C_{\rm cond}(z)dz \simeq C_*\left(1 - \frac{h}{2l_{\rm sed}}\right). \tag{2.4}$$

When $h \ll l_{\rm sed}$, the characteristic mass-diffusion time is $\tau_D \simeq h^2/(\pi^2 D)$ [18]. The substitution of the measured values of the diffusion coefficient $D = 2.2 \times 10^{-7}$ cm^2/s [12] and $h = 2$ mm gives $\tau_D \approx 5$ h, whereas the thermal diffusion time $\tau_T \simeq h^2/(\pi^2\kappa)$, on substitution of the temperature diffusivity coefficient $\kappa = 1.48 \times 10^{-3}$ cm^2/s, hardly reaches 3 s. Thus, the equilibrium temperature gradient $dT/dz = -\Delta T/h$ is settled in the layer about 6000 times faster than the concentration gradient (2.3).

Let us now take into account the Ludwig-Soret effect of thermal diffusion. The density of the matter flux,

$$\mathbf{j} = C\mathbf{u} - D(\nabla C + S\nabla T) \tag{2.5}$$

(S denotes the Soret coefficient), consists of the diffusion part caused by the concentration and temperature gradients and the regular flux due to the gravitational sedimentation of particles. The Archimedean force $\Delta\rho V\mathbf{g}$ and the Stokes drag coefficient $3\pi\eta d$ give rise to the downward particle movement with the velocity

$$\mathbf{u} = \Delta\rho V\mathbf{g}/(3\pi\eta d) = -(D/l_{\rm sed})\,\mathbf{e}. \tag{2.6}$$

Here, η designates the fluid viscosity and the unit vector $\mathbf{e}$ is aligned with the z axis.

In accordance with the Einstein formula, the particle diffusion coefficient is inversely proportional to the nanoparticle diameter d:

$$D = k_B T/(3\pi\eta d). \tag{2.7}$$

Substituting $\mathbf{u}$ from Eq. (2.6) into Eq. (2.5) gives the expression

$$\mathbf{j} = -D[\nabla C + S\nabla T + (C/l_{\rm sed})\,\mathbf{e}], \tag{2.8}$$

where the first term represents the diffusion flux, the second term the thermodiffusion flux, and the third term can be treated as a *barodiffusion* flux [20]: $-D(C/l_{\rm sed})\mathbf{e} = D(C/p)\nabla p$.

We presuppose the small variations in the fluid density ρ,

$$\rho(z) = \rho(1 - \alpha\delta T + \beta\delta C) \tag{2.9}$$

due to deviations of the temperature T and concentration C, respectively, from their mean values $\overline{T}$ and $\overline{C}$. The linear thermal expansion coefficient α and solutal expansion coefficient β,

$$\alpha = -\frac{1}{\rho}\frac{\partial\rho}{\partial T}, \quad \beta = \frac{1}{\rho}\frac{\partial\rho}{\partial C}, \tag{2.10}$$

are positive for the colloid mixture under study.

Convection in a colloidal mixture is described in the Boussinesq approximation by the set of equations which includes the continuity equation for the incompressible medium, the Navier-Stokes equation, the heat conductivity equation, and the diffusion equation for concentration field [4,20]:

$$\nabla\cdot\mathbf{v} = 0. \tag{2.11a}$$

$$\frac{\partial\mathbf{v}}{\partial t} + (\mathbf{v}\cdot\nabla)\mathbf{v} = -\nabla p + P\nabla^2\mathbf{v} + P(R\delta T - B\delta C)\mathbf{e}, \tag{2.11b}$$

$$\frac{\partial\delta T}{\partial t} + (\mathbf{v}\cdot\nabla)\delta T = \nabla^2\delta T, \tag{2.11c}$$

$$\frac{\partial\delta C}{\partial t} + (\mathbf{v}\cdot\nabla)\delta C = L\left[\nabla^2\left(\delta C + \psi\frac{R}{B}\delta T\right) + l^{-1}\frac{\partial\delta C}{\partial z}\right]. \tag{2.11d}$$

Here $l = l_{\rm sed}/h$ is the dimensionless sedimentation length. In Eqs. (2.11), we apply the following scales: length h, time h^2/κ, velocity κ/h, temperature ΔT, concentration $C_* h/l_{\rm sed}$, and pressure $\rho\kappa^2/h^2$. Notably, this time scale differs from one employed in [13]. Later on (Sec. IV) we discuss traveling-wave regimes of convection and compare the results obtained with the results [22] for the wave regimes in molecular binary mixture convection, where the thermal time scale $\tau = h^2/\kappa$ was used. For the layer depth $h = 2$ mm and the temperature diffusivity coefficient $\kappa = 1.48 \times 10^{-3}$ cm^2/s, it appears that the time scale is $\tau \simeq 27$ s.

Dimensionless equations (2.11) contain two control parameters,

$$R = \frac{\alpha g\Delta T h^3}{\nu\kappa}, \quad B = \frac{\beta g C_* h^4}{\nu\kappa l}, \tag{2.12}$$

which are the Rayleigh number and the Boltzmann (or barometric) number, respectively. The material parameters, the Lewis number $L = D/\kappa$, the Prandtl number $P = \nu/\kappa$, and the separation ratio $\psi = (\beta/\alpha)S$, are introduced in Eqs. (2.11), ν denotes the coefficient of kinematic viscosity.

We consider the case of heating from below. The horizontal boundaries at $z = 0, 1$ are taken to be no slip, isothermal, and impenetrable so that there

$$\mathbf{v} = 0, \quad \frac{\partial\delta C}{\partial z} + \psi\frac{R}{B}\frac{\partial\delta T}{\partial z} + \frac{C}{l} = 0, \qquad \delta T(z=0) = 1, \quad \delta T(z=1) = 0. \tag{2.13}$$

We emphasize that contrary to pure thermodiffusion stratification the boundary conditions (2.13) contain the total

concentration $C = \overline{C} + \delta C$ and the derivative of the concentration deviation δC.

The dimensionless temperature and concentration gradients related to the conductive state are as follows:

$$d(\delta T_{\rm cond})/dz = -1, \quad d(\delta C_{\rm cond})/dz = -C_{\rm cond}/l + \psi\frac{R}{B}. \tag{2.14}$$

Upon substitution of the dimensionless concentration of the conductive state $C_{\rm cond}(z) \simeq l - z$ into (2.14) and taking into account that $z/l \ll 1$, we obtain

$$d(\delta C_{\rm cond})/dz \simeq -1 + \psi\frac{R}{B}. \tag{2.15}$$

III. LINEAR THEORY

In this section, the linear stability theory is used to analyze the stability of the quiescent state of a colloidal-mixture layer. Assuming that small perturbations of vertical velocity component $w = (\mathbf{v}\cdot\mathbf{e})$, temperature θ, and concentration φ depend on time and horizontal coordinates as $\exp[\lambda t + i(k_x x + k_y y)]$, we write Eqs. (2.11) as

$$(D^2 - k^2)[P(D^2 - k^2) - \lambda]w - Pk^2(R\theta - B\varphi) = 0, \tag{3.1a}$$

$$(D^2 - k^2 - \lambda)\theta + w = 0, \tag{3.1b}$$

$$L\left[(D^2 - k^2)\left(\varphi + \psi\frac{R}{B}\theta\right) + D\varphi/l\right] - \lambda\varphi + \left(1 - \psi\frac{R}{B}\right)w = 0, \tag{3.1c}$$

where $D = d/dz$ and $k^2 = k_x^2 + k_y^2$. A solution to this set of equations should satisfy the boundary conditions imposed on the confining rigid impenetrable planes:

$$z = 0; 1: \quad w = Dw = \theta = 0, \tag{3.2a}$$

$$D\varphi + \psi\frac{R}{B}D\theta + \varphi/l = 0. \tag{3.2b}$$

A. Long-wave instability

To study the spectra of disturbance increments and to find the stability threshold in the long-wave limit, when $k \to 0$, we represent the solution of Eqs. (3.1) as

$$w(z) = \exp(\lambda t)\sum_{n=0}^{\infty} k^{2n} W_n(z),$$
$$\theta(z) = \exp(\lambda t)\sum_{n=0}^{\infty} k^{2n} \vartheta_n(z), \tag{3.3}$$
$$\varphi(t) = \exp(\lambda t)\sum_{n=0}^{\infty} k^{2n} X_n(z), \quad \lambda = \sum_{n=0}^{\infty} k^{2n}\lambda_n.$$

We assume that the sedimentation parameter is $l^{-1} = O(1)$, and therefore the gravity segregation term in Eq. (3.2b) is retained to the next order in asymptotic expansions, i.e., the diffusive and thermodiffusive fluxes are dominant.

Substituting expansions (3.3) into system (3.1) and matching the factors at the identical degrees of k^2, we derive the equation systems for determining approximate solutions of different orders. To the leading order in k, the boundary conditions take the form

$$z = 0; 1: \quad W_n = DW_n = \vartheta_n = 0, \tag{3.4a}$$

$$DX_n + \psi\frac{R}{B}D\vartheta_n = 0. \tag{3.4b}$$

In the zeroth order of approximation to k^2, the following system is derived:

$$\lambda_0 W_0 = PW_0^{\rm IV}, \quad \lambda_0\vartheta_0 - W_0 = \vartheta_0'', \quad \lambda_0 X_0 = L\left(X_0'' + \psi\frac{R}{B}\vartheta_0''\right). \tag{3.5}$$

This implies that $\lambda_0 = 0$, $\vartheta_0 = 0$, $W_0 = 0$, and that X_0 is the only nonzero function (yet it may be unity, i.e., $X_0 = 1$).

In the first order of approximation, the functions W_1,ϑ_1,X_1 are governed by the following system of equations:

$$W_1^{\rm IV} = -B, \tag{3.6a}$$

$$\vartheta_1'' - W_1 = 0, \tag{3.6b}$$

$$\lambda_1 = L\left(X_1'' + \psi\frac{R}{B}\vartheta_1''\right) - L + \left(1 - \psi\frac{R}{B}\right)W_1. \tag{3.6c}$$

The correction λ_1 is obtained as a result of integration (3.6c) across the layer:

$$\lambda_1 = -L + \left(1 - \psi\frac{R}{B}\right)\int_0^1 W_1\, dz. \tag{3.7}$$

Explicit expressions for W_1 and λ_1 are derived using the boundary conditions

$$W_1 = -\frac{B}{24}(z^4 - 2z^3 + z^2), \quad \lambda_1 = -L - \left(1 - \psi\frac{R}{B}\right)\frac{B}{720}. \tag{3.8}$$

Thus, the stability boundary ($\lambda_1 = 0$) can be represented as

$$R = \frac{720L + B}{\psi}. \tag{3.9}$$

Notably, Eq. (3.9) indicates that long-wave convective instability is observed both in the molecular binary-mixture layer and in the colloidal-mixture layer. The long-wave instability boundary obtained for the molecular, nonstratified ($B = 0$) binary-mixture layer with thermodiffusion [4], can be derived from Eq. (3.9). Since the typical colloid mixture is characterized by the Lewis number (L) of the order of 10^{-4}, it is evident that for the mean concentration $\overline{C} > 1\%$, the Boltzmann number exceeds 100 [13], and the relation $720L \ll B$ holds accurately. Therefore the long-wave convective threshold is expressed as

$$R \cong \frac{B}{\psi}. \tag{3.10}$$

In Ref. [13], expressions (3.9) and (3.10) were derived from the approximate solutions obtained by the Galerkin method. The analysis presented in this section shows correctness of the results of [13] in the general case.

B. Stability boundaries

Linear analysis of the basic state stability relative to disturbances with an arbitrary wave number is carried out by solving the spectral-amplitude problem. The numerical procedure is based on a shooting (sequential) method applying the orthogonalization scheme for integration [21].

In Fig. 1, the critical Rayleigh number R_c, the frequency of neutral oscillations ω, and the critical wave number k_c, which are dependent on the level of gravitational stratification (the Boltzmann number B), are presented for two cases: (i) the absence of thermodiffusion $\psi = 0$ and (ii) anomalous thermodiffusion with $\psi = -0.8$ at two values of the Prandtl number $P = 5.5$ and $P = 100$. The increase of the Boltzmann number B leads to the growth of both the critical

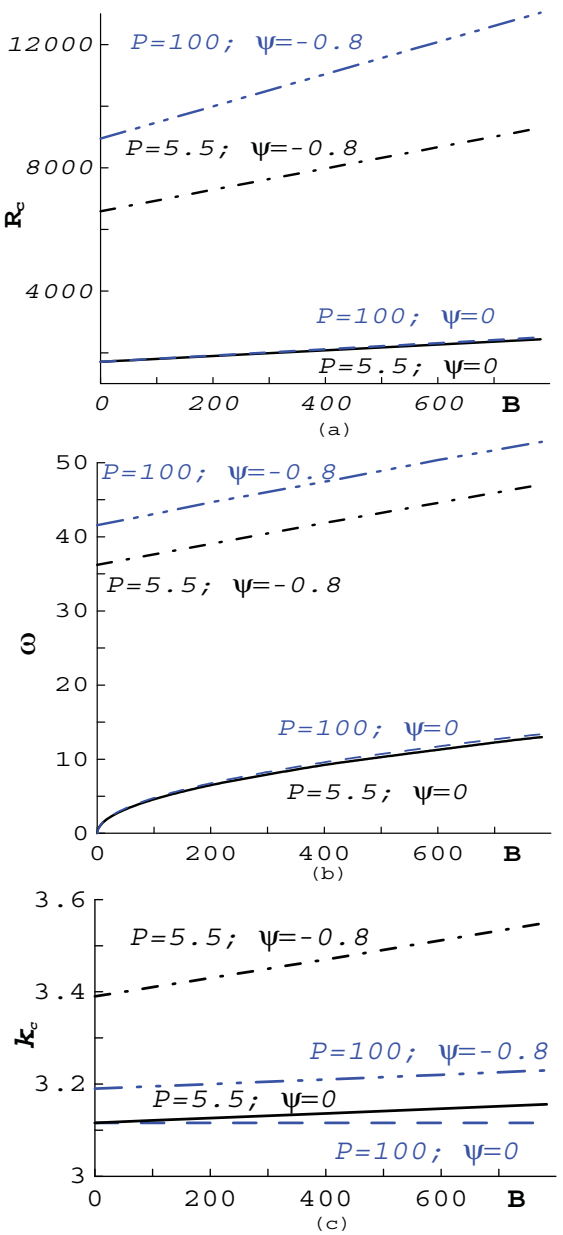

FIG. 1. (Color online) The minimum of the Rayleigh number (a), corresponding frequency value (b), and critical wave number (c) as functions of the Boltzmann number at $L = 1.5 \times 10^{-4}$, $l = 30$.

Rayleigh number R [Fig. 1(a)] and the frequency of neutral oscillations ω [Fig. 1(b)]. The critical wave number k is either constant ($P = 100, \psi = 0$) or a slightly growing function of B [Fig. 1(c)]. The maximum increase of the critical wave number k_c is 4.5% in the considered range $0 < B < 800$.

The Rayleigh number and frequency ω obey the following dependence on B [Figs. 1(a) and 1(b)]:

$$R = R_0 + a(P,\psi)B, \tag{3.11a}$$

$$\omega^2 = c^2(P,\psi) + b^2(P,\psi)B, \tag{3.11b}$$

where R_0, a, b, and c are the fitting coefficients (see Table I). In the absence of thermodiffusion ($\psi = 0$) c vanishes, and the frequency ω depends on the Boltzmann number in accordance with the square root law

$$\omega = b(P)\sqrt{B}. \tag{3.12}$$

In the case of $\psi = -0.8$ the relation $c \gg b$ holds and the linear law $\omega(B)$ is valid:

$$\omega = c + \frac{b^2}{2c}B. \tag{3.13}$$

This behavior is illustrated by Fig. 1(b).

In Ref. [13] the approximate analytical dependencies

$$R_G = \frac{28 f_2(f_1 f_3 + k^2 P B)}{k^2(27 f_3 + 28 P \psi f_2)}, \tag{3.14a}$$

$$\omega_G^2 = \frac{f_1(27k^2 B - 28\psi f_1 f_2)}{(27 f_3 + 28\psi P f_2)}P, \tag{3.14b}$$

$$f_1(k) = 10 + k^2, \quad f_2(k) = 504 + 24k^2 + k^4, \quad f_3(k) = f_1(f_1 + 2) + P f_2 \tag{3.14c}$$

were obtained using the Galerkin approach with

$$w = w_0\left(z^2 - \tfrac{1}{4}\right)^2, \quad \theta = \theta_0\left(z^2 - \tfrac{1}{4}\right).$$

Here, the subscript "G" denotes the Galerkin-type results. The form of Eq. (3.14a) slightly differs from expressions (27) in [13]. This difference is attributed to the alternative time scale used in this study.

As seen from Table I, the numerical results [Fig. 1, Eqs. (3.11)–(3.13)] are in good accordance with the results obtained by the Galerkin method (3.14).

Indeed, one can derive the dependencies $R_G(B)$ and $\omega_G^2(B)$ at the critical value of the wave number k_c for $B = 0$ [Table I, Fig. 1(c)]:

$$R_G = R_G^0 + a_G B, \tag{3.15a}$$

$$\omega_G^2 = c_G^2 + b_G^2 B. \tag{3.15b}$$

As can be seen from Table I, the inequality $c_G \gg b_G$ holds when $\psi = -0.8$. Using the Taylor-series expansion, the linear dependence

$$\omega_G = c_G + \frac{b_G^2}{2c_G}B \tag{3.16}$$

is derived for $P = 5.5$ and $P = 100$. This result is consistent with the data illustrated by Fig. 1(b) (dot-dashed lines) and summarized in Table I (c line).

TABLE I. Comparison of numerical results with results obtained by the Galerkin technique.

	$\psi = 0, P = 5.5$	$\psi = 0, P = 100$	$\psi = -0.8, P = 5.5$	$\psi = -0.8, P = 100$
$k_c(B = 0)$	3.116	3.116	3.39	3.19
R^0	1708	1708	6592	8946
R^0_G	1750	1750	7181	10024
a	0.93	1.01	3.45	5.23
a_G	0.95	1.03	3.83	5.90
b	0.463	0.478	1.076	1.130
b_G	0.459	0.479	1.000	1.171
c	0	0	36.2	41.7
c_G	0	0	37.6	43.85

It should be pointed out that linear stability of equilibrium sharply increases as the denominators in Eq. (3.14c) tend to zero. The heated from below, colloidal-mixture layer with a fully developed conductive concentration profile is stable relative to small perturbations when

$$\psi < \psi_* = -\frac{27 f_3}{28 f_2 P} \cong -1, \tag{3.17}$$

and this is supported by the experimental results ([17], Fig. 1).

The parameter l, responsible for sedimentation in the gravitational field, is of great importance to the nonlinear evolution of colloidal-mixture characteristics (see Sec. IV). However, the numerical results obtained by the shooting method have indicated that its influence on the stability boundaries is insignificant. In a wide range of the parameter l values ($5 < l < 1000$) the Rayleigh number changes very poorly; for example, we have $R = 2079.41$ at $B = 399$ and $R = 2436.63$ at $B = 783$. This result can be explained as follows. In the mechanical equilibrium state (2.14), the parameter l is related to the formation of a concentration gradient. The analysis of the behavior of small disturbances on the stability boundary is governed by the equations containing the concentration gradient in an explicit form. Thus, the diffusion term of the equation for concentration can be ignored because of the extremely small values of the Lewis number (3.1c).

IV. NONLINEAR ANALYSIS

In laboratory experiments dealing with different kinds of thermophilic nanoparticles [17], the permanent oscillatory convection appeared when the definite threshold, not coincident with that predicted by the linear stability theory, was exceeded. It was shown that this threshold decreased as the absolute value of the thermodiffusion parameter $|\psi|$ decreased, and in the absence of thermodiffusion it reached the critical value, which was greater than the convection instability threshold for a quiescent horizontal liquid layer $R^0_c = 1707.8$. In our opinion, this result can be attributed to the effect of colloid stratification in the gravity field. Therefore, the Ludwig-Soret effect is further neglected ($\psi = 0$).

Equations (2.11), which describe two-dimensional convection in the form of y-axial rolls, are solved numerically taking into account gravitational stratification and assuming that thermodiffusion may be ignored. To this end, we introduce the stream function field Ψ and the vorticity field φ, which are velocity related as

$$\mathbf{v} = \left(\frac{\partial \Psi}{\partial z}, 0, -\frac{\partial \Psi}{\partial x}\right), \quad \varphi = (\nabla \times \mathbf{v})_y. \tag{4.1}$$

We also use here the full concentration field $C = \overline{C} + \delta C$. Then the system of partial differential equations (2.11) takes the form

$$\varphi = \nabla^2 \Psi, \tag{4.2a}$$

$$\frac{\partial \varphi}{\partial t} + \frac{\partial \Psi}{\partial z}\frac{\partial \varphi}{\partial x} - \frac{\partial \Psi}{\partial x}\frac{\partial \varphi}{\partial z} = P\nabla^2 \varphi - P\left(R\frac{\partial \delta T}{\partial x} - B\frac{\partial C}{\partial x}\right), \tag{4.2b}$$

$$\frac{\partial \delta T}{\partial t} + \frac{\partial \Psi}{\partial z}\frac{\partial \delta T}{\partial x} - \frac{\partial \Psi}{\partial x}\frac{\partial \delta T}{\partial z} = \nabla^2 \delta T, \tag{4.2c}$$

$$\frac{\partial C}{\partial t} + \frac{\partial \Psi}{\partial z}\frac{\partial C}{\partial x} - \frac{\partial \Psi}{\partial x}\frac{\partial C}{\partial z} = L\left(\nabla^2 C + \frac{1}{l}\frac{\partial C}{\partial z}\right). \tag{4.2d}$$

The conditions imposed on the horizontal boundaries describe the impermeability of the plates and the absence of slip along them:

$$z = 0;1: \quad \Psi = 0, \quad \frac{\partial \Psi}{\partial z} = 0, \tag{4.3a}$$

$$\frac{\partial C}{\partial z} + \frac{C}{l} = 0. \tag{4.3b}$$

We consider the developed, nonlinear colloid-mixture flow in a horizontal layer heated from below. Rigid boundaries of the layer are kept at different constant values of temperature:

$$\delta T(z = 0) = 1, \quad \delta T(z = 1) = 0. \tag{4.4}$$

Periodic boundary conditions, $f(x,z,t) = f(x + \lambda, z, t)$, imposed on the lateral sides of a convection cell, are assigned to all variable fields $f = \Psi, \varphi, \delta T, C$, with $\lambda = 2$.

To solve the system of equations (4.2) in the general case, the finite-difference technique is applied. The evolution equations are approximated using an alternating-direction implicit scheme of the second order with central differences for spatial derivatives and one-sided right differences for time derivatives. The Poisson equation for the stream function was worked out by means of an iterative method of successive overrelaxation at each time step. Typically, a regime of steady-state, finite-amplitude convective oscillations obtained

at a particular set of parameters was used as an initial condition for a run at a different set of parameters. All calculations were executed on a grid of 124 × 81 nodes. Further mesh refinement did not provide a significant improvement in the evaluation of oscillation characteristics and showed no relevant differences.

A. Diagnostic tools

To assess the heating intensity, the reduced Rayleigh number $r = R/R_c^0$ is used, where R_c^0 is the critical Rayleigh number for the onset of pure-liquid convection with the corresponding wave number k_c^0. The linear stability theory predicts $R_c^0 = 1707.8$ and $k_c^0 = 3.116$. However, to compare the numerical results presented in this paper with the well-known experimental, analytical, or numerical ones of other authors, we scale R by the threshold $R_c^0 = 1705.6$ obtained using our numerical code.

To monitor the process, the following convection characteristics are used: (1) the maximum value of the vertical velocity component in the $x - z$ cross section perpendicular to the roll axis

$$w_{\max}(t) = \max_{x,z} w(x,z,t); \tag{4.5}$$

(2) the value of the vertical velocity component in the reference point x_0,z_0 of the convection cell

$$w_{\rm loc}(t) = w(x_0 = \lambda/4, \quad z_0 = 1/2, t); \tag{4.6}$$

and (3) the lateral phase velocity $v_{\rm ph}$ of w, which is measured by the time derivative of node locations of $w(x,z,t)$ at the midheight of the liquid layer $z = 1/2$:

$$v_{\rm ph} = \frac{dx_{(w=0)}}{dt}. \tag{4.7}$$

For all traveling waves with the lateral periodicity $\lambda = 2\pi/k$, the phase velocity $v_{\rm ph}$ is used to identify the frequency of the modulated traveling wave as

$$\omega_{\rm TW} = v_{\rm ph} k. \tag{4.8}$$

We analyze the evolution of the spatial variance of the concentration field. To this end, we monitor the mixing number describing the concentration difference in the convective cell:

$$M = \sqrt{\langle (\delta C)^2 \rangle / \langle (\delta C_{\rm cond})^2 \rangle}. \tag{4.9}$$

Here the $\langle \cdots \rangle$ implies a space-average value over the layer.

In the quiescent layer ($\mathbf{v} = 0$), the gravity-induced conductive concentration profile $C_{\rm cond}(z) = l - z$ varies from $l - 1$ at the top to l at the bottom with $\langle (\delta C_{\rm cond})^2 \rangle = 1/12$.

In the conductive state, M equals 1 by definition. When the convection excitation threshold is exceeded, advective mixing reduces the mean square deviation $\langle (\delta C)^2 \rangle$ of the concentration field; the better colloid is mixed due to advection, the closer M approaches the limit $M = 0$ for a perfectly mixed fluid.

B. Numerical results: A traveling-wave regime

Let us consider the nonlinear evolution of convective patterns in a colloidal binary mixture layer heated from below. In calculations, we employed the following geometric and material parameters: $l = 30$, the Lewis number $L = 1.5 \times 10^{-4}$,

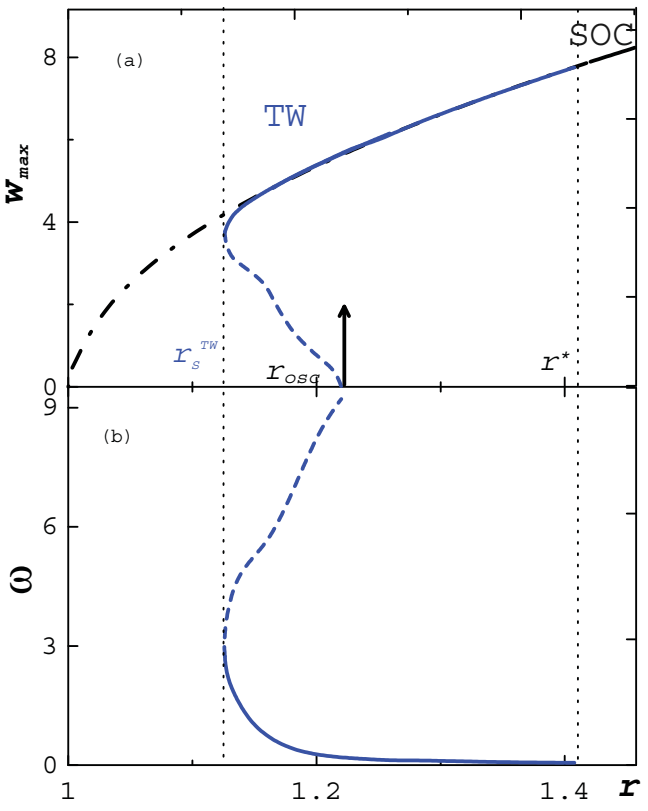

FIG. 2. (Color online) The bifurcation diagram of laterally extended convective states with wave number $k = \pi$ in colloid mixture as functions of the reduced Rayleigh number r. Full (dashed) thick lines relate to $w_{\max}$ (a) and the frequency ω (b) of stable (unstable) solution in a gravity stratified colloid mixture. The thin dash-dotted line corresponds to homogeneous liquid. $L = 1.5 \times 10^{-4}$, $P = 5.5$, $\psi = 0$, $B = 399$, and $l = 30$.

and the Prandtl number $P = 5.5$. This set of parameters is characteristic for experimentally realizable colloidal mixtures, and it is the same as that used in [12].

We are concerned with the properties of the traveling-wave (TW) mode as well as the oscillatory transients into the TW or the conductive state in the case of the Boltzmann number $B = 399$.

Figure 2 represents the bifurcation diagram of various convective regimes obtained numerically. It illustrates the dependencies of the maximum vertical velocity $w_{\max}$ and the oscillating frequency ω on the reduced Rayleigh number. The solid and dashed lines correspond to the colloidal binary mixture, and the dot-dashed line corresponds to the homogeneous one-component fluid.

According to the linear stability theory, when the heating intensity increases quasistatically, the onset of convection occurs via a Hopf bifurcation at the value of reduced Rayleigh number $r_{\rm osc} = 1.217$ and is characterized by the Hopf frequency $\omega_H(k = \pi, r_{\rm osc}) = 9.21$.

On the other hand, as evidenced by the nonlinear numerical simulations, a convection in a colloid-mixture layer demonstrates a pair of the symmetry degenerated left- and right-handed traveling-wave solutions, bifurcating backward from the conductive state at $r_{\rm osc} = 1.218$, which is in good agreement with the predictions of the linear theory

[see Fig. 1(a), the lower branch for TW solutions]. At $r_S^{\mathrm{TW}} = 1.125$, the traveling waves gain stability via a saddle-node bifurcation. For $r < r_S^{\mathrm{TW}}$, the colloid-mixture convection decays and the system turns to the conductive state. The branch of stable TWs ends at $r^* = 1.42$, and the branch of stable stationary overturning convection (SOC) appears. Thus, the highly developed, nonlinear traveling-wave convection is stable in the interval of reduced Rayleigh numbers $r_S^{\mathrm{TW}} < r < r^*$ [the upper branch for solutions in Fig. 1(a)].

The bifurcation behavior of the nonlinear TW solutions is also evident from Fig. 2(b) that illustrates the dependence $\omega(r)$. This frequency reaches its maximum $\omega_H = 9.20$ at the Hopf bifurcation critical point r_{osc}. When the reduced Rayleigh number r is decreased from r_{osc}, the frequency values corresponding to unstable TW regimes [see the lower, dashed branch in Fig. 2(a)] decrease as well. At the saddle point, r_S^{TW}, the TW frequency is about three times less than the Hopf frequency $\omega_S^{\mathrm{TW}} = 2.72$. Then an increase of r fits with the upper TW branch in Fig. 2(a), and the TW frequency falls to zero at r^* corresponding to loss of stability of the SOC mode in a parity-breaking bifurcation.

When $r > r^* = 1.42$, the evolution of perturbation against the equilibrium temperature and concentration fields brings about the formation of a stationary overturning convection pattern. This SOC regime is settled in the colloid-mixture layer after the transient standing-wave regime, and the concentration field within the cell in the final stage of evolution has become almost homogeneous. This type of a transition in the colloidal liquid mixture is studied in detail, taking into account gravitational stratification [13], or thermodiffusion [14].

Note that the bifurcation diagram of TW solutions in the gravity stratified colloid mixture (Fig. 2) is qualitatively similar to the bifurcation diagram of TW regimes in the molecular binary mixture with negative thermodiffusion coupling [6,22]. On the other hand, both TW and SOC modes in a molecular binary mixture have the mirror-glide (MG) symmetry [5,6]:

$$f(x,z;t) = -f(x+\lambda/2, 1-z; t), \tag{4.10}$$

where f denotes $\Psi, \varphi, \delta T$, or δC. In the case of colloid mixture the terms $l^{-1}(\partial C/\partial z)$ in Eq. (4.2d) and C/l in Eq. (4.3b) break this symmetry.

C. Transient behavior

The result of the evolution of initial perturbation depends on the heating intensity r. If the value of the Rayleigh number belongs to the interval $r_{\mathrm{osc}} < r < r^*$, then the small oscillating disturbances grow and the traveling-wave regime is formed in the layer upon the completion of the transient stage. Similar behavior has also been observed for the molecular-mixture layer [22].

We consider the nonlinear evolution of convective structures producing the traveling-wave flow pattern at $r = 1.294$. At the first stage, the standing-wave regime is settled as a result of the oscillatory perturbation growth [Fig. 3(a), $t < t_a$]. The points in the convective cell, where the stream function takes its maximum $\Psi_{\max}$ or minimum $\Psi_{\min}$ values, interchange their positions each half period of oscillations

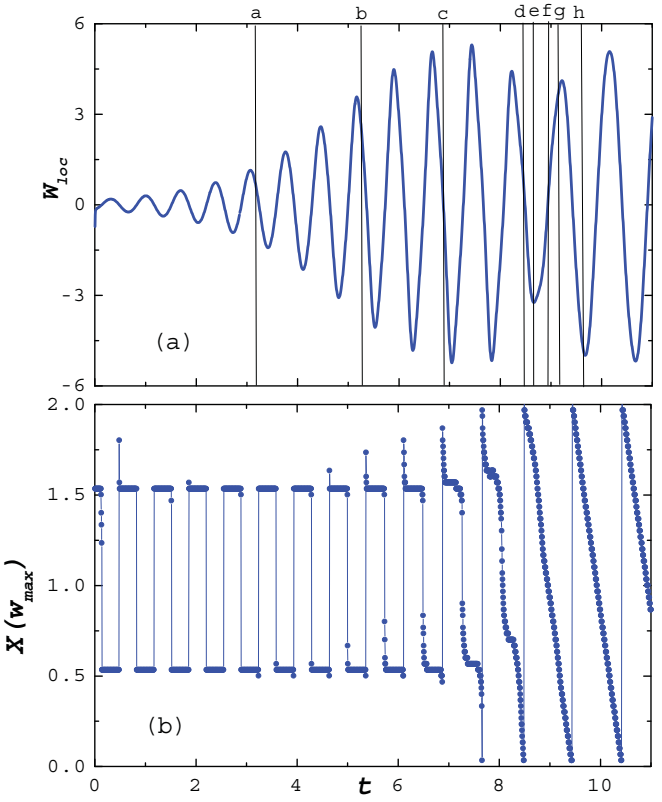

FIG. 3. (Color online) The evolution of $w_{\mathrm{loc}}(t)$ (a) and the coordinate of vertical velocity nod $x_{(w=0)}$ (b) at the beginning stage of the transition from the quiescent binary mixture to the TW regime. The specific time moments are labeled by lines a, b, c, d, e, f, g and h. $L = 1.5 \times 10^{-4}$, $P = 5.5$, $\psi = 0$, $l = 30$, $B = 399$, and $r = 1.294$.

[see Fig. 3(b), $t < t_a$]:

$$\begin{aligned} x_{\Psi_{\max}}(t) &= x_{\Psi_{\max}}(t + \pi/\omega) + \lambda/2, \\ x_{\Psi_{\min}}(t) &= x_{\Psi_{\min}}(t + \pi/\omega) - \lambda/2. \end{aligned} \tag{4.11}$$

These points correspond to the nodes of the vertical velocity component $x_{w=0}$. The wave amplitude—the maximum intensity of the convective motion—goes up with time [see Fig. 3(a) for w_{loc}]. With all this going on the fields of stream function, temperature and concentration change harmonically with the spatial period $L = 2\pi/k$. The snapshots of the concentration field in the transient regime are presented in Fig. 4 and correspond to the time moments, which are labeled "a–h" in Fig. 3.

At the next stage, the intensity of convective motion increases and the concentration field gets spatial anharmonicity [Figs. 4(b)–4(f)]. This effect is most noticeable at the time moments, when the velocity is close to zero. At a certain point, the standing-wave regime becomes unstable, then collapses, and after the relatively fast transient stage the traveling-wave regime develops.

When $t > t_b$, the horizontal movement appears in the layer [see Fig. 3(b)]. The spatial symmetry inherent in a standing-wave regime is lost [Fig. 4(c)], and the concentration field undergoes qualitative rearrangement [Figs. 4(e)–4(h)]. Within the time interval $t_g < t < t_h$, the traveling-wave mode

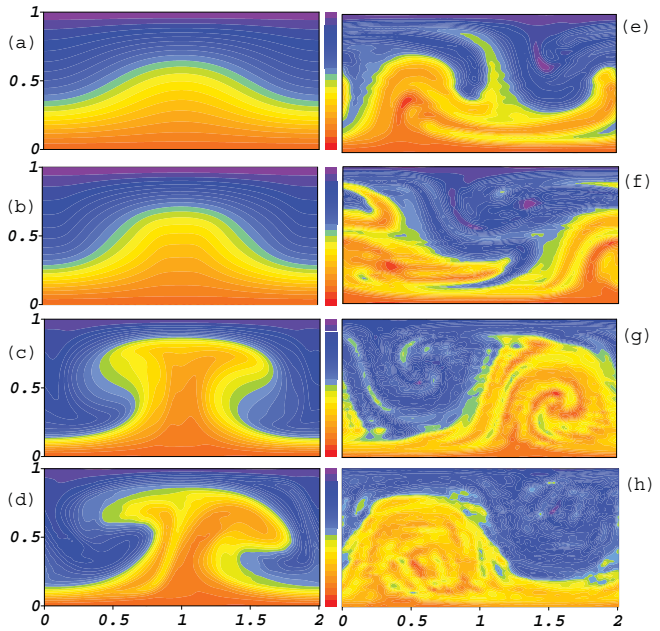

FIG. 4. (Color online) Snapshots of the concentration field through the transition from the quiescent binary mixture to the TW at $r = 1.294$. The times "a–h" are indicated by vertical lines in Fig. 3. In the color online version the vertical color bars show the coding in the conductive state with $C_{\rm cond}(z)$ varying linearly from 30 at the bottom to 29 at the top for $l = 30$. $L = 1.5 \times 10^{-4}$, $P = 5.5$, $\psi = 0$, and $B = 399$.

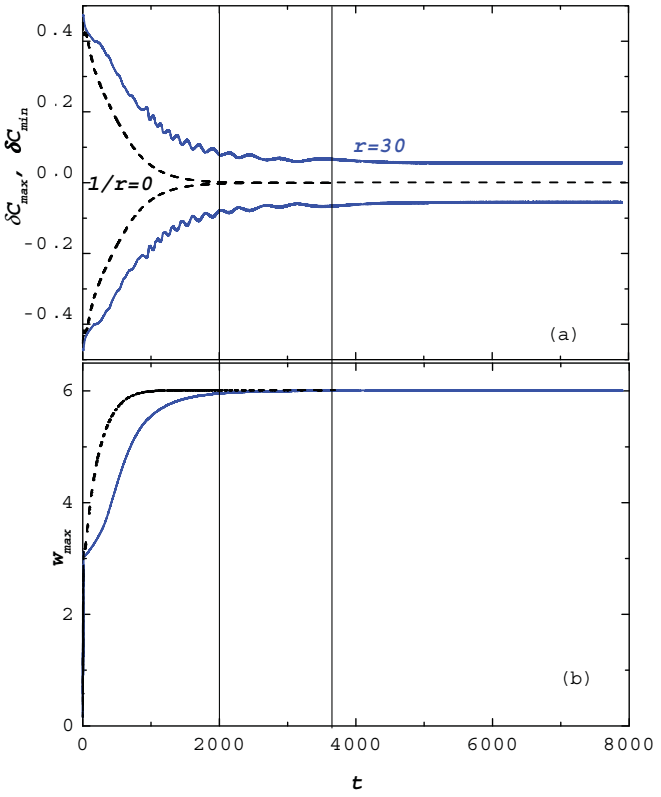

FIG. 5. (Color online) The time dependencies of maximum $\delta C_{\rm max}$ and minimum $\delta C_{\rm min}$ of concentration (a) and vertical velocity $w_{\rm max}(t)$ (b) in the case of gravity segregation $l = 30$ (solid blue lines) or in the case of its absence ($1/l = 0$) (dashed black lines). $L = 1.5 \times 10^{-4}$, $P = 5.5$, $\psi = 0$, $B = 399$, and $r = 1.246$.

is characterized by the constant phase velocity, and the sharp boundary layers are formed [Fig. 4(h)]. Such a field pattern reproduces a transition to the traveling-wave flow structure taking place in the molecular mixtures stratified due to the negative Soret coupling [22]. It should be mentioned that the rearrangement of the standing-wave mode into the traveling-wave regime lasts over approximately the same time period, $t \sim 1.5$, as in the case of the colloidal mixture stratified by the gravity field, and in the molecular mixture stratified by thermodiffusion. The point is that the transition is dependent on the character of convective mixing and independent of the specificity of the diffusive process. So the term with the Lewis number L as a coefficient can be neglected in the right-hand side of the evolutionary equation for concentration (4.2). The difference between the maximum and minimum values of the colloid-mixture concentration within the transient stage does not practically change. The mixing parameter at this moment $M \simeq 0.90$ is close to its maximum value.

At $r = 1.294$, the time period required for setting the traveling-wave flow pattern is $\Delta t_{\rm TW} \approx 11$, which corresponds to the dimensional value of 5 min. The lesser the critical level exceeding $r - r_{\rm osc}$, the slower small perturbations develop, and the more time is needed to increase the standing-wave amplitude and to turn to the traveling-wave regime.

Further evolution of the traveling-wave mode becomes apparent on the diffusion time scales. Figure 5 illustrates the effect of smoothing the concentration profile inhomogeneities $\delta C_{\rm max}$ and $\delta C_{\rm min}$ due to the convective mixing. At $r = 1.246$, the initial (maximum) concentration deviation in the convective cell $\delta C_{\rm max}$ decreases [Fig. 5(a)], and the maximum convective vertical velocity $w_{\rm max}$ (the intensity of convective motion) increases and reaches the stationary level [Fig. 5(b)]. At this time the dynamic balance is established in the colloidal mixture between the sedimentation level in the gravitational field and the convection mixing. For a specified set of parameters, the stationary level of the concentration difference is approximately five times less than that of the motionless mixture. The time of setting a new concentration difference in the traveling-wave regime is $t = 3600$ ($\approx$27 h). To make sure of such traveling-wave properties, we have extended the dimensionless simulation period to $t = 8000$. This does not change the concentration difference or the stream function field. Thus such traveling-wave patterns can be recognized as stable.

For comparison, the transient behavior is modeled for the idealized case of cancellation of sedimentation in the gravitational field as soon as the nonuniform concentration profile is formed in the layer: $B \neq 0$ and $1/l = 0$ (Fig. 5). Hence the convective motion brings a colloidal mixture into the homogeneous state with zero difference between the maximum and minimum concentration values. The concentration difference reaches the zero level during the time period $t = 2000$, which is shorter than that at $1/l \neq 0$. Obviously, this can be attributed to the fact that sedimentation does not interfere with the diffusive mixing of the colloidal mixture.

The concentration field in the stable TW solution is strongly anharmonic (Fig. 6). In the case of $r = 1.246$ the vertical

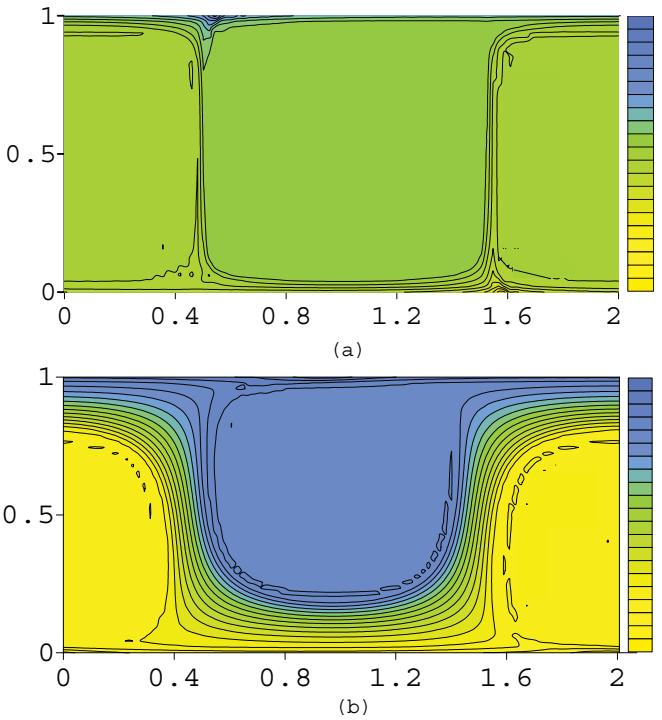

FIG. 6. (Color online) Snapshots of the concentration field in the final stage of the TW. (a) $r = 1.246$ and (b) $r = 1.126$. The vertical color bars in the color online version show the coding with $C_{\max} = 29.602$ and $C_{\min} = 29.398$. $L = 1.5 \times 10^{-4}$, $P = 5.5$, $\psi = 0$, $B = 399$, and $l = 30$.

velocity w is relatively large and therefore convective mixing is strong. The mixing parameter is close to zero, $M = 0.04$. The concentration in every point of the convective cell practically equals its mean value $C \approx \overline{C} = 29.5$ [Fig. 6(a)] except narrow regions near boundaries of the layer. Maximum concentration deviation $\delta C_{\max}$ equals 0.053.

The concentration field of TW solution at a lower value of $r = 1.126$ (slightly above the saddle-node bifurcation point r_S^{TW}) is more inhomogeneous than that in the previous case [Fig. 6(b)]. This pattern is characterized by the higher values of the mixing parameter $M = 0.21$ and $\delta C_{\max} = 0.102$.

Reaching the Rayleigh number value r_S^{TW}, the dynamic balance is broken in favor of sedimentation, the convective motion settles down, and the system passes into the mechanical equilibrium state. The corresponding transition is shown in Fig. 7 for $r = 1.123$. At the first stage, when $t \leqslant 2100$, the convective mixing intensity ($w_{\max}$) decreases slowly, and the difference in the concentration values $\delta C_{\max}$ increases very slowly. The dimensional time of the oscillations, $t \simeq 5.67 \times 10^4 c$, corresponds to the typical time of transient oscillations observed in the experiment [17]. At the next stage, when $2100 < t < 2600$, the vertical convective velocity quickly goes to zero, and then the sedimentation in the gravitational field leads to the increase in maximum of concentration deviation ($\delta C_{\max}$). It is clear that the final stage of this segregation process on the background of a quiescent binary mixture is the equilibrium concentration distribution.

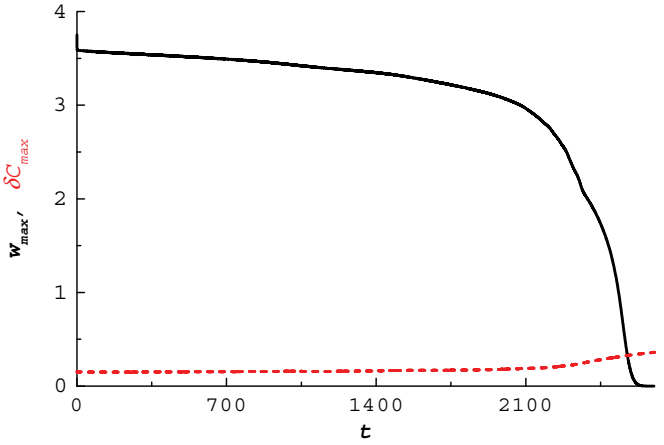

FIG. 7. (Color online) The time dependence of maximum vertical velocity $w_{\max}(t)$ (4.5) (solid black line) and concentration difference $\delta C_{\max}$ (dashed red line) in the transient from the TW regime to binary mixture equilibrium state. $r = 1.123$, $L = 1.5 \times 10^{-4}$, $P = 5.5$, $\psi = 0$, $B = 399$, and $l = 30$.

In the presence of thermodiffusion the following effects might be expected in the layer with colloid mixture when heating from below. According to [13], the oscillatory instability exists in the case of $\psi < B/R_c^0$, that is, $\psi < B/1708$. Therefore, in the presence of gravity stratification stable TW regimes in colloids might be expected even in the case of the positive Soret coupling. In the opposite case of the negative Soret coupling, sedimentation and thermodiffusion act in the same direction, opposing the convective instability, and the higher Rayleigh number is necessary to support the stable (permanent) TW solution. Similar transient behavior of a colloid mixture has been observed in [17].

V. CONCLUSION

We have investigated the onset of convection in the horizontal, colloidal binary mixture layer subjected to gravitational segregation, as well as the bifurcations of traveling roll flow patterns and spatiotemporal behavior of these periodic regimes.

Based on the calculated results, we have theoretically substantiated a loss of stability of the quiescent colloidal-mixture layer due to the growth of oscillatory perturbations, long-wavelength or cellular, in a wide range of values for the separation ratio, sedimentation length, and the Prandtl number. The explicit relations between the convection thresholds and the dimensionless parameters of the problem have been derived. We have observed that the convection thresholds and flow evolution on the thermal time scale are practically independent of the sedimentation length. However, this parameter plays the main role in the TW pattern formation, which develops on the diffusive time scales.

To illustrate the typical temporal oscillations of the flow intensity and the concentration field structure, the nonlinear dynamics of the traveling-wave mode is represented by a set of consecutive contour maps. The transitions between the conductive state and the traveling-wave flow pattern have been studied in detail.

It has been shown that the obtained nonlinear results and the predictions of the linear theory concerning the convection thresholds are in good agreement. We have found numerically that the unstable TW solution, occurring in the colloidal-mixture layer stratified by gravity, bifurcates backward out of the conductive state, and the stable TW solution exists in some heating interval. It has been found that the bifurcation diagram obtained for the TW regimes in the gravity stratified colloid mixture looks like the diagram for the molecular binary mixture with the negative Soret coupling.

Selection of a dissipative structure realizable in a colloidal binary mixture layer is rather sensitive to the morphological conditions of the generated concentration field, which could have demonstrated the spatial anharmonicity within convective cells. This result can be used to control the heat mass transfer characteristics of nonequilibrium colloidal systems.

ACKNOWLEDGMENTS

This work was partially supported by the Israeli Ministry of Science through Grant No. 3-5799 and the Russian Foundation for Basic Researches (Projects No. 07-01-96037, No. 09-01-92472-MHKC, and No. 10-01-96037).

[1] *Multifield Problems in Solid and Fluid Mechanics*, edited by R. Helmig, A. Mielke, and B. I. Wohlmuth, Lecture Notes in Applied and Computatuional Mechanics, Vol. 28 (Springer-Verlag, Berlin, 2006).

[2] I. D. Morrison and S. Ross, *Colloidal Dispersions: Suspensions, Emulsions, and Foams* (Wiley Interscience, New York, 2002).

[3] M. C. Cross and P. C. Hohenberg, Rev. Mod. Phys. **65**, 851 (1993).

[4] J. K. Platten and J. C. Legros, *Convection in Fluids* (Springer-Verlag, Berlin, 1984), p. 680.

[5] W. Barten, M. Lücke, W. Hort, and M. Kamps, Phys. Rev. Lett. **63**, 376 (1989).

[6] M. Lücke, W. Barten, P. Büchel, C. Fütterer, St. Hollinger, and Ch. Jung, in *Evolution of Structures in Dissipative Continuous Systems*, edited by F. H. Busse and S. C. Müller, Lecture Notes in Physics, Vol. m55 (Springer, Berlin, 1998), p. 127.

[7] R. W. Walden, P. Kolodner, A. Passner, and C. M. Surko, Phys. Rev. Lett. **55**, 496 (1985).

[8] I. Rehberg and G. Ahlers, Phys. Rev. Lett. **55**, 500 (1985).

[9] G. Ahlers and I. Rehberg, Phys. Rev. Lett. **56**, 1373 (1986).

[10] E. Moses and V. Steinberg, Phys. Rev. Lett. **57**, 2018 (1986).

[11] P. Kolodner, Phys. Rev. A **46**, 1739 (1992).

[12] R. Cerbino, A. Vailati, and M. Giglio, Phys. Rev. E **66**, 055301(R) (2002); Philos. Mag. **83**, 2154 (2003).

[13] M. I. Shliomis and B. L. Smorodin, Phys. Rev. E **71**, 036312 (2005).

[14] B. Huke, H. Pleiner, and M. Lücke, Phys. Rev. E **75**, 036203 (2007).

[15] M. C. Kim, J. S. Hong, and C. K. Choi, AIChE J. **52**, 2333 (2006).

[16] M. C. Kim, C. K. Choi, and J. K. Yeo, Phys. Fluids **19**, 084103 (2007); M. C. Kim and C. K. Choi, Phys. Rev. E **76**, 036302 (2007).

[17] G. Donzelli, R. Cerbino, and A. Vailati, Phys. Rev. Lett. **102**, 104503 (2009).

[18] More precisely [19], $\tau_D = \frac{h^2}{\pi^2 D}(1 - \ln\frac{\pi^2}{8} + \frac{h}{12l} + \cdots)$, thus for $h/l \ll 1$ one has $\tau_D = 0.790h^2/(\pi^2 D)$.

[19] Yu. L. Raikher and M. I. Shliomis, J. Magn. Magn. Mater. **122**, 93 (1993).

[20] L. D. Landau and E. M. Lifschitz, *Course of Theoretical Physics*, Vol. 6 (Pergamon Press, Oxford, 1993).

[21] U. M. Ascher, R. M. M. Mattheij, and R. D. Russell, in *Numerical Solution of Boundary Value Problems for Ordinary Differential Equations*, Prentice Hall Series in Computational Mathematics (Prentice-Hall, Englewood Cliffs, NJ, 1988).

[22] C. Fütterer and M. Lücke, Phys. Rev. E **65**, 036315 (2002).